Luminosity functions of AGN and their emissivity of UHECRs and neutrinos

Henrik Døvle Andrews
Norwegian university of Science and Technology

January 11, 2024

Abstract

Motivated by the search for the source of ultra-high-energy cosmic rays (UHECRs) and high energy neutrinos, one will in this report discuss the evolution of different classes of Active Galactic Nuclei (AGN), a potential candidate for high energy particles, and calculate their emissivity of UHECRs and neutrinos based on the x-ray luminosity. This emissivity will then be compared to the emissivity of UHECRs and neutrinos as seen by ground based telescopes here on Earth. In addition, one will also discuss the population evolution and population distribution over luminosity of the different classes. To do this one will consider the luminosity functions of our different classes generated by surveys looking in the x-ray band. The results of the luminosity functions shows that the distribution of AGN over luminosity can be separated into two classes. Most jet-dominated AGN show a preferred luminosity around which we find the most AGN, while most non-jet dominated AGN show an increase in numbers towards lower luminosity and a break luminosity where their slope index change. For the redshift evolution one also find a difference between the two classes. The total population for most jet-dominated AGN show a peak at earlier redshift than non-jet-dominated AGN. Both results have an interesting exception which are the Bl lacs who are increasing in numbers with lower redshift and also show an increase in numbers towards lower luminosities but belong to the class of jet-dominated AGN. The second part of the analysis in this report focuses on the emissivity UHECRs and neutrinos. One shows that assuming a similar luminosity between x-ray, UHECRs, and neutrinos, almost all classes of AGN can alone produce the observed diffuse flux of UHECRs and neutrinos. One concludes that one needs a better correlation model between x-ray and the particles to make a more accurate estimate of the emissivity of UHECRs and neutrinos. In addition, one wants a model that includes the observational properties of AGN, most notably jet orientation.

Acknowledgments

I would like to thank my supervisor, Professor Foteini Oikonomou, for her guidance and help throughout this project. I would also like to thank my fellow students for their help and support.

Contents

1 Introduction 7

1.1 Motivation and background . . . 7

1.2 Outline . . . 7

2 The ever-expanding Universe 8

2.1 Cosmological parameters . . . 8

2.2 Shape of the Universe . . . 8

2.3 Redshift . . . 9

2.4 Comoving distance . . . 10

2.5 Luminosity distance . . . 11

3 High energy particles 12

3.1 Acceleration of high energy particles . . . 12

3.2 UHECRs . . . 14

3.2.1 Production and Energy loss . . . 14

3.2.2 Detection . . . 15

3.2.3 Emissivity estimates . . . 15

3.3 Neutrinos . . . 17

3.3.1 Production and Energy loss . . . 17

3.3.2 Detection . . . 18

3.3.3 Emissivity estimates . . . 19

4 Active galactic nuclei 21

4.1 AGN structure and classification . . . 22

4.1.1 Accretion disk . . . 22
4.1.2 Corona and X-ray emission . . . 24
4.1.3 Broad and narrow line region . . . 24
4.1.4 Dust torus . . . 25
4.1.5 Jets . . . 25
4.2 Types of AGN . . . 26

5 Luminosity functions **28**
5.1 X-ray LF . . . 29

6 Luminosity function results **33**
6.1 Luminosity distribution . . . 33
6.2 Density distribution . . . 36
6.3 Expected luminosity . . . 38

7 AGN power injection estimation **40**
7.1 UHECRs emissivity . . . 40
7.2 Neutrino emissivity . . . 41

8 Conclusion **45**
8.1 Summary . . . 45
8.2 Future outlook . . . 46

List of Figures

1 Hillas criterion for proton (blue line) and iron (red line) accelerated up to $10^{20} eV$ and $10^{21} eV$ respectively. Image taken from Kotera and Olinto 2011 13

2 The diffuse flux of UHECRs as measured by the Pierre Auger Observatory and the Telescope Array. The flux is separated into galactic and extra galactic sources where the total spectrum follows the black dots. Image taken from Abdul Halim et al. 2023 16

3 The IceCube neutrino observatory. The detector is located at the South Pole and is a large block of ice instrumented with photomultiplier tubes. Image taken from Andeen and Plum 2019 19

4 The diffuse flux of neutrinos as measured by the Ice Cube observatory. The y-axis on the left image is the number of events per bin. The flux is separated into contributions from atmospheric neutrinos and astrophysical neutrinos. The right image is the model astrophysical flux as measured by ICE CUBE. Images taken from Abbasi et al. 2022 20

5 AGN unification 23

6 Luminosity distribution for the different classes of AGN. The different classes are defined in the title as well as the chosen LF model. 34

7 Density distribution for the four different classes of AGN. The different classes are defined in the title as well as the chosen LF model. 36

8 Expected luminosity and emissivity for the different classes of AGN. 39

9 UHECR emissivity for the different classes of AGN. 40

10 Neutrino emissivity for the different classes of AGN. 42

11 Diffuse neutrino flux for the different classes of AGN. 43

List of Tables

1 The model parameters for the astrophysical flux of UHECRs as measured by the Pierre Auger Observatory and the Telescope Array. 16

2 The model parameters for the astrophysical flux of neutrinos as measured by the Ice Cube observatory. 20

3 X-ray LF parameters, a, normalized by a factor of 10^{-7}, b, normalized by a factor of 10^{44} c, has more factors that do not fit in the table, $z_{c2} = 3$, $\alpha_2 = -0.1$, $L_{c2} = 10^{44}$, $v_3 = -6.2$, $\beta = 0.84$ 29

4 Luminosity range for different models, the luminosity range is given in log10. 29

1 Introduction

1.1 Motivation and background

Cosmic rays and neutrinos have become an important tool for studying the Universe. Their unique properties allow them to probe different regions better than regular photons and are therefore a great complementary tool in observational astronomy. Although the information gain of detecting Cosmic rays and neutrinos are great, they are not without their challenges, especially when one moves into higher energies where the fluxes are low.

The biggest challenge relating to ultra-high-energy cosmic rays (UHECR) and high energy neutrinos is their source. Both of these particles are thought to be produced in the most energetic events/objects in the Universe, and as such the search for these sources are of great interest. One of the candidates is Active Galactic Nuclei (AGN). These are some of the most energetic objects in the Universe, powered by accretion of matter onto supermassive black holes. AGN are a fairly new object in astronomy, and one can separate them into several subclasses based on orientation, all with different potential to produce UHECRs and neutrinos.

1.2 Outline

The main goal of this report is to discuss the evolution of different classes of AGN, and calculate their emissivity of UHECRs and neutrinos based on the x-ray luminosity. This emissivity will then be compared to the emissivity of UHECRs and neutrinos as seen by ground based telescopes here on Earth. To do this one will consider the distribution of the different classes in both Luminosity and redshift using luminosity functions generated by surveys looking in the x-ray band.

One starts in chapter 2 with a brief introduction to distance measures in cosmology. In chapter 3 one will discuss UHECRs and neutrinos, how they are produced, how they interact when propagating through the Universe, how they are detected and importantly the estimate of their respective emissivity. Chapter 4 will discuss AGN, their structure, and their subclasses. In chapter 5 one introduce Luminosity functions, and the functional forms of the Luminosity functions used in this report along with their parameters. Then, in chapter 6 one will discuss the results of the Luminosity functions. In chapter 7 one will discuss the results of the emissivity calculations, and compare them to the results of the Luminosity functions. Finally, in chapter 8 a conclusion and future outlook is given.

2 The ever-expanding Universe

To investigate sources very far away from an observer it is important to understand the influence this distance has on the desired observables. Therefore, in astrophysics and astronomy in general there are distances created to take into account the effects of an expanding Universe. This chapter draws heavily from Hogg 2000.

2.1 Cosmological parameters

A reasonable place to start is with the Hubble constant H_0. This parameter sets the recession speed of a point at proper distance d and the current position via the relation $v = H_0 d$. The subscript 0 refers to the present epoch signifying that H_0 is not static but changes with time. The precise value of H_0 is quite debated, so it's commonly expressed in a parameterised form,

$$H_0 = 100 \frac{\mathrm{km}}{\mathrm{s}} \frac{1}{\mathrm{Mpc}} h.$$

The parameter h is a dimensionless number that according to current knowledge can take the value between 0.5 to 0.8 reflecting the range of answers collected from recent work.

Beyond its basic definition, H_0 also allows for the derivation of two significant cosmic scales:

Hubble Time (t_H) : Defined as the inverse of H_0, t_H provides an estimate of the age of the Universe. It sets a scale for the time since the Big Bang, assuming the Universe has been expanding at a constant rate. The equation $t_H = 1/H_0 \approx 14 \quad$ Billion years offers a way to approximate this expansion timescale.

Hubble Distance (D_H) : This is a measure of the distance. Calculated as $D_H = c/H_0 \approx 4.4 \quad$ Gly, where c is the speed of light, it represents a critical boundary in observational cosmology.

2.2 Shape of the Universe

The shape and expansion of the Universe are central themes in cosmology, but first one needs to define the structure of the Universe and its contents. In this report and many articles, the Universe is often explored through the lens of the flat Lambda Cold Dark Matter (ΛCDM) model. This model, widely accepted in contemporary cosmology, provides a framework for understanding the Universe's composition and its expansion dynamics by assuming as the name suggests no curvature. In the ΛCDM model, two key parameters are important: the mass density of the Universe, ρ_0, and the cosmological constant, Λ. These parameters, which evolve, are a part of defining the metric tensor in general relativity, thereby allowing us to model the curvature of the Universe based on its initial conditions. These parameters are often expressed as dimensionless variables:

$$\Omega_m = \frac{8\pi G\rho_0}{3H_0^2}$$

$$\Omega_\Lambda = \frac{\Lambda c^2}{3H_0^2}$$

Here, Ω_m represents the matter density parameter, encompassing both ordinary (baryonic) matter and dark matter. Ω_Λ, on the other hand, corresponds to the density parameter associated with the cosmological constant, which is often interpreted as dark energy.

In general, one has a third density parameter Ω_k which defines the curvature of space-time and the relationship between these parameters is expressed as:

$$\Omega_m + \Omega_\Lambda + \Omega_k = 1$$

In a flat Universe, one has $\Omega_k = 0$ and the Universe is dominated by dark energy and dark matter. The model used in this report and the papers used in the following chapters is the flat ΛCDM model where the parameters take the values of $\Omega_\Lambda = 0.7$ and $\Omega_m = 0.3$. These values align with current observational data.

2.3 Redshift

Redshift is defined as the fractional Doppler shift of emitting light. The Doppler effect is a known effect on different observables in the Universe where the relative motion of sources to observers will impact the observable. The redshift is quantified for a light source as

$$z = \frac{\nu_e}{\nu_o} - 1 = \frac{\lambda_o}{\lambda_e} - 1 \tag{1}$$

Here o refers to the observed quantity and e the emitted. Due to the expansion of the Universe the light emitted from a distant source will be increasingly redshifted the further away it is. In these scenarios the redshift serves as a distance measure, allowing us to deduce distances to faraway objects.

2.4 Comoving distance

Comoving distance is an important concept in cosmography, acting as a standard unit for various distance measurements in the Universe. This distance, often termed the line-of-sight distance for an observer on Earth, remains constant even as objects expand with the Hubble flow. To calculate the total comoving distance (D_c) to an object, one integrates the differential comoving distances (δD_c) along the line of sight, starting from redshift $z = 0$ to the object. This integration necessitates consideration of the Universe's parametric composition and the δD_c is expressed as

$$\delta D_c = \frac{D_H}{E(z)} dz, \tag{2}$$

where the function $E(z)$ is defined as

$$E(z) = \sqrt{\Omega_m (z+1)^3 + \Omega_k (1+z)^2 + \Omega_\Lambda}. \tag{3}$$

Here, $E(z)$ incorporates the density parameters previously discussed and the redshift z. It also relates to the Hubble constant observed by a hypothetical observer at redshift z, expressed as $H(z) = H_0 E(z)$.

One then calculates the comoving distance D_c from

$$D_c = D_H \int_0^z \frac{dz}{E(z)} \tag{4}$$

In addition to the line of sight, one needs to define the transverse comoving distance D_m. This distance relates two points in the night sky at the same redshift separated by an angle $d\theta$. The actual distance between them $d\theta D_m$ will then vary depending on the curvature of the Universe. This relationship is summarized in the following equation which accounts for different geometries,

$$D_m = \begin{cases} D_h \frac{1}{\sqrt{\Omega_k}} sinh(\frac{\sqrt{\Omega_k} D_c}{D_H}) & \text{if } \Omega_k > 0 \\ D_c & \text{if } \Omega_k = 0 \\ D_h \frac{1}{\sqrt{|\Omega_k|}} sin(\frac{\sqrt{|\Omega_k|} D_c}{D_H}) & \text{if } \Omega_k < 0 \end{cases}$$

The different cases correspond to hyperbolic, flat, and spherical geometry respectively. The true nature of the Universe is still unknown, but recent observations indicate a flat Universe.

2.5 Luminosity distance

The luminosity distance D_l is defined through the relation between the bolometric flux F of a source and its bolometric luminosity L. Bolometric flux is the energy received per unit of time per unit area without any obscuration, while bolometric luminosity is the total energy emitted per unit of time. The luminosity distance is defined as

$$D_l = \sqrt{\frac{L}{4\pi F}} \tag{5}$$

This formula reflects how the observed flux at the observer's location differs based on the distance from the source and the intrinsic luminosity emitted.

It is related to the transverse comoving distance via

$$D_l = (1+z)D_m. \tag{6}$$

If one wants to calculate the spectral flux/ differential flux one needs to take into account a correction. This correction comes from the fact that one is viewing a redshifted object. The object is emitting in a different band than observed. The spectrum of the differential flux F_ν is related to the spectral luminosity via

$$F_\nu = (1+z)\frac{L_{(1+z)\nu}}{L_\nu}\frac{L_\nu}{4\pi D_l^2}. \tag{7}$$

All these equations listed help include the effects of an expanding Universe when astronomers study distant objects and their properties.

3 High energy particles

In this chapter, I will discuss the different types of high-energy particles that are of interest in this paper, i.e. neutrinos and ultra-high energy cosmic rays (UHECRs). I will briefly discuss their generation and how they are detected. Then introduce how they lose energy in their journey to the Earth, and lastly calculate the emissivity of their hypothetical sources from the ground observations here on earth.

3.1 Acceleration of high energy particles

To reach high energy, particles need to be accelerated. Knowing the exact source of acceleration can be difficult if one do not know the source, but one can put constraints on any source given some simple arguments. By arguing that the acceleration needs to be of a certain strength and that the particle being accelerated needs to stay confined within the accelerating region for long enough one can create an upper band. This is called the Hillas criterion introduced in Hillas 1984, and is a way of estimating the maximum energy a particle can reach in a given source.

For relativistic particles with charge Z and energy ϵ in a magnetic field of strength B one can define the Larmor radius

$$R_L = \frac{\epsilon}{ZB} \tag{8}$$

By arguing that the confinement of a particle to an accelerating region is the same as setting the Larmor radius equal to the size of the source. One can easily derive the maximum achievable energy for a particle as follows.

$$\epsilon_{max} = ZBR \tag{9}$$

Via this method, one can estimate the potential candidates that can produce the observed high-energy particles. The criterion works as an upper boundary of acceleration sources since it does not account for energy loss in the acceleration process or any type of interaction that one could expect to be in turbulent environments. In figure 1 one can see the different candidates for the acceleration of two different ions, protons, and iron. One of the candidates is the AGN, which is the focus of this paper.

The method of acceleration can be important for different sources, and therefore it seems useful to

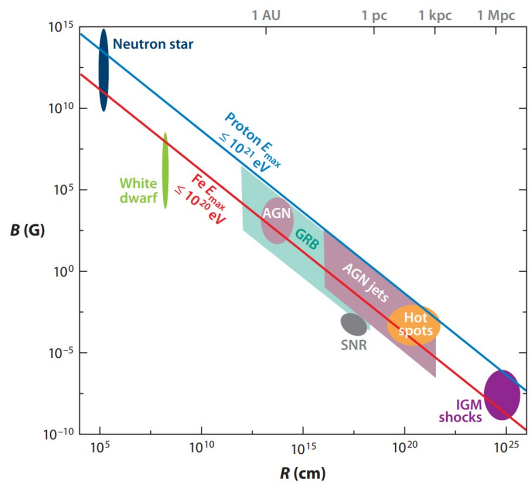

Figure 1: Hillas criterion for proton (blue line) and iron (red line) accelerated up to $10^{20}eV$ and $10^{21}eV$ respectively. Image taken from Kotera and Olinto 2011

briefly go through some of them.

One-shot acceleration: In the presence of an ordered electric field, one can continuously accelerate charged particles. This could be the feature of some astrophysical objects such as neutron stars and black holes.

Diffusive acceleration/ Fermi acceleration In regions where one has high variability in the magnetic field strength, one can accelerate particles in steps. This is called diffusive acceleration and the most common way of this happening is through first and second-order Fermi acceleration. The second-order Fermi acceleration is the simplest and is based on the fact that particles can gain energy by bouncing back and forth between magnetic clouds which act as mirrors. This is a stochastic process and the average energy gain can be shown to be proportional $(\frac{v}{c})^2$. Here v is the speed of the cloud and c is the speed of the particle. This is a slow process due to the scarcity of clouds, and therefore it is not a preferred method. The first-order Fermi acceleration happens when particles collide with strong shock fronts. These shock fronts can be quite a bit faster than the interstellar clouds and when a particle moves through the shock it gains energy proportional to $\frac{v}{c}$. In addition to this, there is a probability that the particle will stay in the accelerating region and experience several accelerations.

By knowing how particles can be accelerated and their potential sources one can continue and look at the two particles in question in this paper. Neutrinos and UHECRs.

3.2 UHECRs

UHECRs are charged particles that are bombarding the Earth with energy exceeding 1 exaelectronvolt (10^{18} eV) Alves Batista et al. 2019. The origin of these particles is still a mystery but due to their high energies, they are thought to be extragalactic in origin. The composition of UHECRs ranges from protons to heavier nuclei such as helium or iron, and when these particles interact with the atmosphere they produce a shower of secondary particles. The air showers could also give extra information such as direction, but due to the nature of UHECRs, the location of their source is difficult to pinpoint. This is because UHECRs are charged particles and therefore are deflected by the magnetic fields they encounter.

3.2.1 Production and Energy loss

The requirements to produce a UHECR are a charged particle and a powerful accelerator. But in order to model them sufficiently one needs to take into account their journey to the Earth. Both during the acceleration and during the journey to Earth, the UHECRs will lose energy. The important parameters for this energy loss are its composition and its environment. In addition, as mentioned before, the interstellar magnetic field will also deflect the particles and therefore the direction of the particle will be changed. These effects are important parameters since they limit the distance a particle can travel before it loses too much energy, and therefore limits the local volume in which high energy cosmic rays can be produced. Here I will briefly discuss the different energy loss mechanisms.

Photo-pair production

$$p + \gamma \rightarrow p + e^- + e^+ \tag{10}$$

For UHECRs, the most dominant sink of energy when under a certain energy threshold is the Bethe-Heitler process. In this process, a proton of sufficient energy interacts with the photon field in its vicinity and produces a pair of electrons and positrons. The photon field can vary from the cosmic microwave background to the generated field from different sources. The energy loss of this process is quite small $\sim \frac{2m_e}{m_p} = 10^{-3}$ of the original energy of the proton, but the process is very common, and therefore it is a significant energy loss over time.

Photo-Pion production

$$p + \gamma \rightarrow \Delta^+ \rightarrow (p + \pi^0) \quad \text{or} \quad (\pi^+ + n) \tag{11}$$

Given enough energy the proton can interact with the photon field and produce a delta resonance. This resonance can then decay into a pion and a proton or a pion and a neutron. It is important since it also puts an upper limit on the UHECR energy for intergalactic particles. This limit, called the Greisen-Zatsepin-Kuzmin (GZK) limit comes from the UHECRs interacting with the cosmic microwave background in this delta resonance process. The limit caps proton energy at 5×10^{19} eV. In this mechanism the original proton loses $m_p/m_\pi \approx 20\%$ of its energy resulting in a quite rapid loss of energy.

3.2.2 Detection

When a cosmic ray hits the atmosphere it will interact with the air molecules and produce a cascade of particles and light that can more easily be detected than the original cosmic ray. In addition, since the UHECR flux at high energy is extremely low (<1 particle per km^2 per year for $E > 10^{19}$) one needs a large area to collect enough data. The largest UHECRs detectors of present are the Pierre Auger Observatory and the Telescope Array.

The Pierre Auger Observatory is located in Argentina and is the largest detector of its kind. It consists of 1660 Cherenkov detectors spread over 3000 km^2 and 27 fluorescence telescopes in four locations. With these instruments, the observatory is very capable of reconstructing the air showers and therefore the energy and direction of the cosmic ray. The observatory has a blind spot in the night sky and therefore the observatory is complemented by the Telescope Array located in Utah. The Telescope Array is a smaller observatory with 507 scintillator detectors and 3 fluorescence telescopes. Combined they have been able to map the full sky of UHECRs.

3.2.3 Emissivity estimates

Now that one reasonably understands the nature of UHECRs one can try to make tangible estimates of the UHECR sources. One such estimate is the emissivity of UHECR sources. The emissivity is a measure of the energy released per unit time per unit volume. The question one can ask is what is the necessary emissivity of UHECRs to explain the observed flux here on Earth? In other words, what is the required energy injection rate of UHECRs?

Via observations from the Pierre Auger Observatory and the Telescope Array, one can observe and model the diffuse flux of UHECRs. The result is an isotropic flux and is represented in Figure 2. The functional form of the flux is a broken power law taken from Collaboration et al. 2017 and is given as

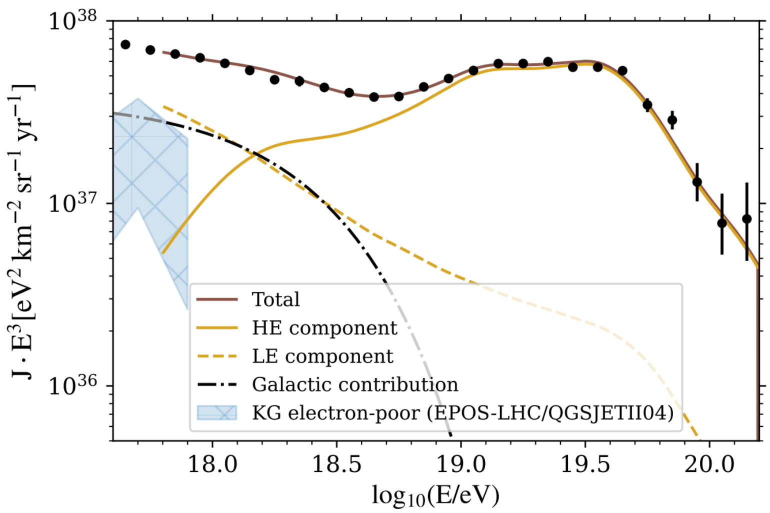

Figure 2: The diffuse flux of UHECRs as measured by the Pierre Auger Observatory and the Telescope Array. The flux is separated into galactic and extra galactic sources where the total spectrum follows the black dots. Image taken from Abdul Halim et al. 2023

J_0	E_{ank}	γ_1	γ_2	γ_d	E_s
3.3×10^{-19}	4.82×10^{18}	3.14	4.2	3.14	4.2×10^{19}

Table 1: The model parameters for the astrophysical flux of UHECRs as measured by the Pierre Auger Observatory and the Telescope Array.

$$J(E_v) = \begin{cases} J_0 \left(\frac{E_v}{E_{\text{ank}}}\right)^{-\gamma_1} \text{if } E_v < E_{\text{ank}} \\ J_0 \left(\frac{E_v}{E_{\text{ank}}}\right)^{-\gamma_2} \left(1 + \left(\frac{E_{\text{ank}}}{E_s}\right)^{\gamma_d}\right) \left(1 + \left(\frac{E_v}{E_s}\right)^{\gamma_d}\right)^{-1} \text{if } E_v \geq E_{\text{ank}} \end{cases} \tag{12}$$

with parameters in table 1.

By separating the flux into contributions from extragalactic sources and galactic sources one can estimate the required energy density in the Universe of extragalactic UHECRs. From here can define an energy loss time for a UHECR as the loss length divided by the speed of light c. The loss length is a measure of the distance a UHECR can travel before its energy drops below a certain threshold, and for our simple analysis, we will use the length of $1Gpc$. This number is comparable in magnitude as found by Stanev 2009 but as the loss length is dependent on initial energy and composition our number will be an approximation. Then the emissivity of UHECRs produced by the sources is the energy density divided by the loss time.

The previous discussion is summarized in the following equation

$$\epsilon_{\text{UHECR}} = \frac{u_{\text{UHECR}}}{t_{\text{loss}}} = \frac{u_{\text{UHECR}}}{D_{\text{loss}}/c} = \frac{4\pi c \int_{E_0}^{E_{\max}} J_{\text{extragalactic}}(E) E dE}{c D_{\text{loss}}} \approx 9 \times 10^{44} \frac{\text{erg}}{\text{Mpc}^3\text{yr}}. \quad (13)$$

Here u_{UHECR} is the energy density of UHECRs, t_{loss} is the energy loss time, D_{loss} is the loss distance, $J(E)$ is the flux of UHECRs, $E_0 = 1$ exaelectronvolt, is the minimum energy of the flux where it is dominated by extragalactic UHECRs, and E_{max} is the maximum energy of extragalactic UHECRs. The value of ϵ_{UHECR} is calculated in the script available on GitHub Andrews 2023 by using data from Auger Collaboration et al. 2017. This emissivity is a crude estimation of the required energy injection rate of UHECRs and is meant to give a rough estimate. The main points of criticism are the estimate of our loss distance which does not include the composition of the UHECRs or its initial energy. Nevertheless, one receives an emissivity comparable to a more thorough analysis from Aab et al. 2020 which received a value of $6 * 10^{44} \frac{\text{erg}}{\text{Mpc}^3\text{yr}}$.

3.3 Neutrinos

The second particle of interest is the neutrino. Neutrinos compared to UHECRs are neutral particles that are produced in various processes in the Universe. The most common and well-known is the fusion reaction in the sun where neutrinos are produced in the pp chain. On the other hand the neutrinos of focus in this paper are high-energy neutrinos that are likely produced in the same sources as the UHECRs.

3.3.1 Production and Energy loss

The production sites of high-energy neutrinos is not clear, but they are thought to be produced in the same sources as UHECRs and in this section, I will go through the most probable way of producing high-energy neutrinos in sources such as AGN.

Hadronic processes:

Hadronic processes can release neutrinos with sufficiently high energy to explain the observations here on Earth. Processes such as nuclear interactions are limited by the binding energy of the nucleus and accelerating a neutrino after its production is difficult. Therefore, a common way of producing the observed neutrinos is through the decay of pions. The most important decay is the decay of charged pions into muons and muon neutrinos as seen in equation 14

$$\pi^+ \rightarrow \mu^+ + \nu_\mu \rightarrow e^+ + \nu_e + \nu_\mu + \bar{\nu_\mu} \quad (14)$$

I will discuss two possible ways of producing these pions in two different environments.

In a proton-rich environment where the protons can accelerate up to high energies, one can produce pions through the following process

$$p + p \to \begin{cases} \pi^+ + n + p \\ \pi^- + \pi^+ + p + p \\ \pi^0 + p + p \end{cases} \tag{15}$$

The energy of these protons at a few GeV is enough to introduce the delta-baryon resonance, and therefore it becomes more complicated. Therefore, the most efficient way of producing pions is through the already seen delta resonance when a proton interacts with a photon, this is seen in equation 11. This process being the cooling process of UHECRs is interesting and indicates that a source that produces high energy neutrinos likely is inhabited by very energetic charged particles.

After having produced the neutrinos it also becomes important to understand their behavior during their travel to Earth. Here I will highlight two points

Neutrino oscillations: In the previous paragraph, I discussed the production of these neutrinos, but not their initial flavor. The pion decay model is known to produce a flavor composition of $\nu_e : \nu_\mu : \nu_\tau = 1 : 2 : 0$. A naive thought would be an identical composition observed on Earth, but sadly this is not the case. The reason for this is that the neutrinos' mass state can oscillate between the different flavors. Therefore, the neutrinos produced in the source will oscillate during their travel to Earth and when they reach us one would expect a uniform mix of the three flavors, $nu_e : \nu_\mu : \nu_\tau = 1 : 1 : 1$.

Energy loss: To model the travel of a neutrino of any flavor one only needs to take into account the interaction of the neutrino with the expanding universe. Since it is so weakly interacting the only source of energy loss the flux of neutrinos will experience is the redshift created by the expansion of the Universe. This redshift is the same as the one discussed in the previous section and the neutrinos behave the same way light does in this manner with a drop in energy proportional to $(1 + z)$.

3.3.2 Detection

Neutrinos are weakly interacting matter particles and therefore are very difficult to detect. This makes them excellent candidates for the study of the Universe since they can travel large distances without interacting, but make them quite difficult to detect with high accuracy. The most famous

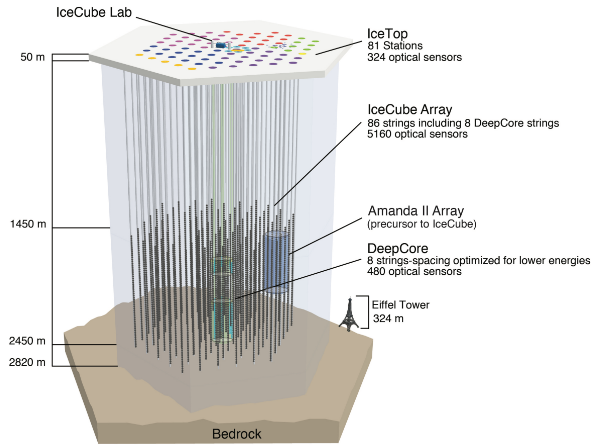

Figure 3: The IceCube neutrino observatory. The detector is located at the South Pole and is a large block of ice instrumented with photomultiplier tubes. Image taken from Andeen and Plum 2019

detector and the one used in this paper is the IceCube neutrino observatory. This detector is precisely what it sounds. It is a large block of ice with a size equal to a square kilometer located at the South Pole. The observatory uses the ice located deep in the South Pole as a giant Cherenkov detector. The ice is instrumented with photomultiplier tubes that can detect the Cherenkov radiation produced by neutrinos interacting with the ice. More precisely the observatory is fitted with 5160 photomultiplier tubes located at a depth of 1450-2450 m. The photomultipliers are divided into 86 strings of 60 modules each. The detector is also complemented by the DeepCore detector which is a denser array of photomultiplier tubes located in the center of the detector. See Figure 3 for a visual representation of the detector. The energy range for this detector is from 10 GeV to 10 EeV. The interaction of neutrinos with the water molecules in the ice can produce charged leptons (muons, electrons or taus). These charged particles if energetic enough will then produce Cherenkov radiation which can be detected by the photomultiplier tubes.

3.3.3 Emissivity estimates

Armed with the required knowledge above one can also make simple arguments for the sources of these neutrinos based on the observed flux here on Earth. The flux used in this paper is the diffuse flux of neutrinos as measured by the Ice Cube observatory. The flux is shown in figure 4. For any calculations, we use the astrophysical flux as modeled as a power law. The power law is of the form

$$\Phi(E) = \Phi_0 \left(\frac{E}{E_0}\right)^{-\gamma} \tag{16}$$

Φ_0	E_0	γ
$6.7 \times 10^{-18} GeV^{-1} cm^{-2} s^{-1} sr^{-1}$	$100 TeV$	2.37

Table 2: The model parameters for the astrophysical flux of neutrinos as measured by the Ice Cube observatory.

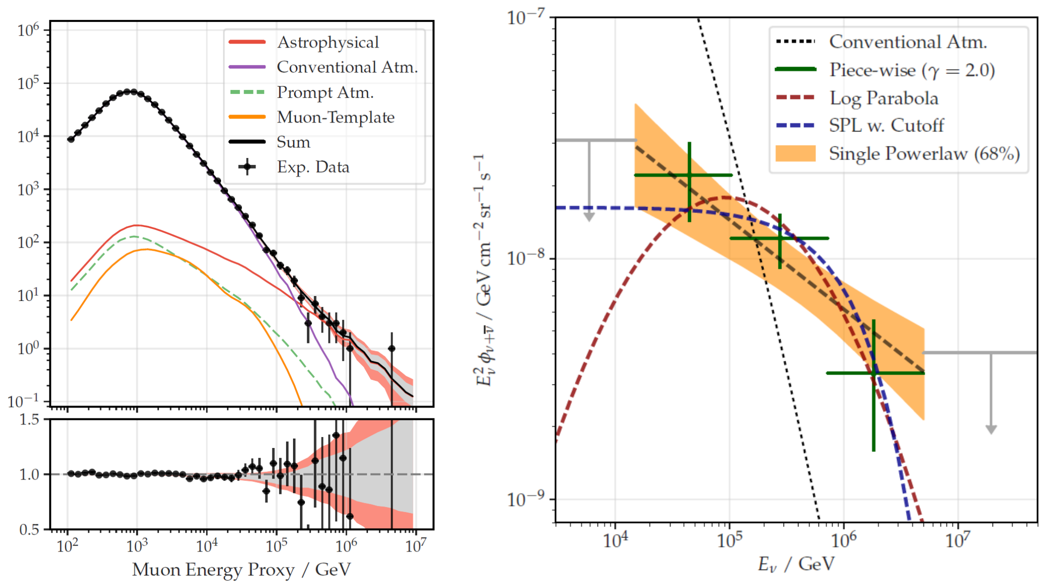

(a) Number of events per bin (b) Modeled Astrophysical flux

Figure 4: The diffuse flux of neutrinos as measured by the Ice Cube observatory. The y-axis on the left image is the number of events per bin. The flux is separated into contributions from atmospheric neutrinos and astrophysical neutrinos. The right image is the model astrophysical flux as measured by ICE CUBE. Images taken from Abbasi et al. 2022

with Φ_0 being the normalization constant, E_0 being the reference energy and γ being the spectral index. The model parameters are seen in table 2 and taken from Abbasi et al. 2022.

The emissivity of neutrinos is calculated in the same way as for UHECRs. The only difference is the loss time. Neutrinos do not lose energy in the same way as UHECRs and therefore the loss distance will be the size of the Universe. The modeled emissivity is then approximately $1.54 \cdot 10^{44} \quad erg/Mpc^3/yr$.

4 Active galactic nuclei

Active Galactic Nuclei (AGN) are an interesting topic in astrophysical studies, and since their discovery, there has been rapid advancement in understanding these phenomena. Today, AGN are known to be among the brightest entities in the night sky, but they only gained significant attention in the early 1950s. This shift occurred with the arrival of new radio observations, which revealed a new type of quasi-stellar object through the discovery of the Quasars.

Initially, these luminous objects, characterized by broad, unidentifiable spectral lines, were enigmatic to scientists. However, with the identification of more sources and their optical parts, it became clear that these were not stars but a distinct class of celestial objects. Furthermore, research done by M. Schmidt on one of the emission lines from Quasar 3C 273 opened the interpretation of these celestial objects. He found that the emission lines of quasars were similar to hydrogen, but were redshifted by a factor of 0.158, an exceptionally high value at the time according to Shields 1999. Observations at the same time also revealed significant variability in quasar luminosity, suggesting that these objects were no larger than one light year across. These observations lead to the speculation of super luminous objects located very far away from Earth. The problem was that such objects had no reasonable explanation at the time.

Observation of the surrounding galaxy of AGN with matching redshift and observation of gravitational lensing cemented the distances of these objects. In addition, the modern view of black holes which had only been a theory in the 1950s came to fruition and the idea of accretion allowed for the modern model of an AGN to be born. This modern perspective views AGN as supermassive black holes that accrete matter from surrounding gas. In addition to this the modern view of AGN also include jets, torus, and different emitting regions that are used to classify AGN.

In the most recent times, a landmark achievement was achieved in March 2021, when scientists associated with the Event Horizon Telescope project presented the first image of the supermassive black hole at the center of the Messier 87 galaxy, located 55 million light-years away. This image, showing a bright ring surrounding a dark central region, aligns with predictions for an accreting supermassive black hole, increasing our confidence in the modern model. In addition, the 2020 Nobel Prize in physics was awarded to Roger Penrose, Reinhard Genzel, and Andrea Ghez for their work on black holes and AGN, further cementing the importance of these objects in modern astrophysics.

4.1 AGN structure and classification

The modern view of AGN is a unified model that combines the different categories of powerful luminous objects cataloged in the mid to late 20th century. These distinctions that astronomers made still have value, but to understand an AGN it is important to get a picture of the unified structure.

An active galactic nucleus is defined as a galaxy center containing a massive accreting black hole. This mass according to Netzer 2015 is defined as $M_{BH} > 10^5 M_\odot$. AGN also have an Eddington ratio exceeding the limit of $L_{\rm AGN}/L_{\rm Edd} = 10^{-5}$, where $L_{\rm AGN}$ is the bolometric luminosity, and $L_{\rm Edd}$ is the Eddington luminosity for a solar composition gas. These definitions help constrain what galaxies might contain an AGN, where it excludes the Milky Way by these criteria, but it fails to capture the full structure definition of an AGN. Therefore, the structure of most AGN will include several of the following components, first summarized then expanded upon:

- A close rotational dominated accretion disc around the SMBH.
- High-density gas clouds that are said to be dust-free moving at high velocities close to the black hole, in the so-called broad line region(BLR)
- Low-density gas clouds that move at lower velocities further away from the black hole in the so-called narrow line region(NLR)
- A structure of dust that is responsible for the obscuration of the central region of the AGN. This is called the torus due to its theorized shape. It lies at a luminosity-dependent distance from the SMBH, but according to Netzer 2015 this is around 0.1 - 10 pc depending on the luminosity.
- A corona of hot electrons that is thought to be responsible for the X-ray emission seen in AGN. This is thought to be located above the accretion disk.
- A relativistic jet that is thought to be powered by the accretion disk. This is not always present but is a common feature of AGN.

The reader is directed to figure 5 for a visual representation of the different components.

4.1.1 Accretion disk

An accretion disk is a natural consequence of the conservation of angular momentum. In the case of infalling matter coming close to a supermassive black hole, the matter could have some

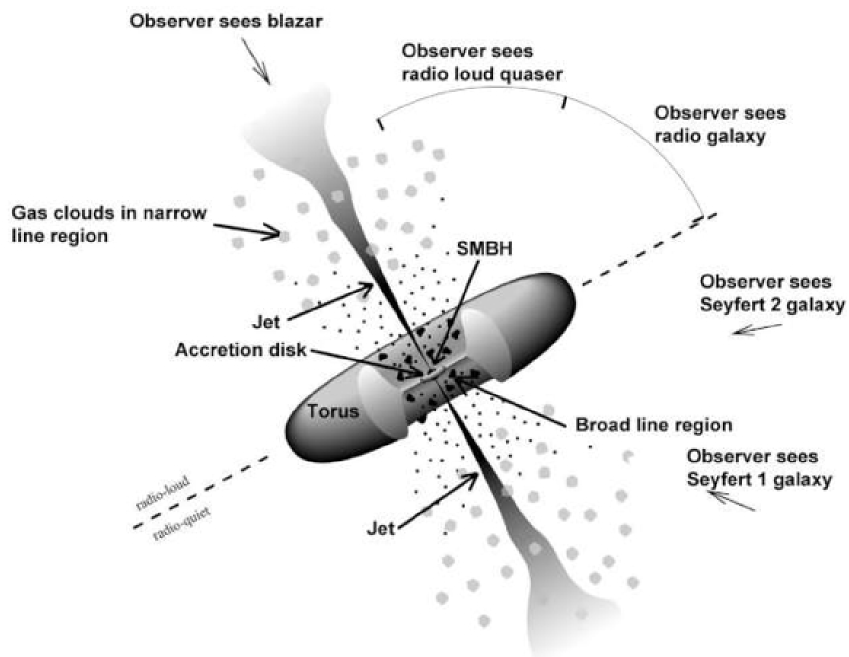

Figure 5: AGN unification

angular momentum. With this the gas should orbit the black hole at some stable distance but, due to radiative processes, fluid viscosity, and gravitational turbulence, the matter will lose angular momentum and spiral inwards. The inward spiral will eventually allow the matter to fall into the black hole. This process of inspiral is what is called accretion and the forces acting on the matter to cause the inspiral will also in the same process heat it up to high energies causing it to radiate. The radiation is closely linked to the infalling matter that is accreted onto the black hole and one can express the total luminosity of the accretion disk as

$$L_{acc} = \eta \dot{M} c^2. \tag{17}$$

Here η is the efficiency of the accretion process, $\dot{M}$ is the mass accretion rate and c is the speed of light.

The efficiency of the accretion disk is a function of the spin of the black hole and the radius of the innermost stable circular orbit (ISCO). The ISCO is a counter-intuitive term in classical mechanics but in general relativity the maximum speed of a particle in addition to an energy term when calculating the orbit set bounds for how close a particle can be to a black hole without spiraling in.

The accretion disk also has a bound for its maximum luminosity. As calculated for stars the Eddington luminosity sets a maximum strength for the radiation pressure of the accretion disk. This is given as

$$L_{Edd} = \frac{4\pi G M m_p c}{\sigma_T} \tag{18}$$

The heating of the accretion disc will lead to thermal radiation from the disc and this radiation will be proportional to the temperature of the disc. This temperature is radially dependent and if one assumes an optically thick but geometrically thin disk also called a Shakura-Sunuaev disk one can express the radiative surface energy flux taken from Dermer and Menon 2009(p. 106) as

$$\frac{dE}{dAdt} = F_{rad}(r) = \frac{3GM\dot{M}}{8\pi r^3}\left(1 - \beta\sqrt{\frac{r_{\mathrm{ISCO}}}{r}}\right) \tag{19}$$

Here β is a constant that relates the fraction of angular momentum captured by the black hole, and r_{ISCO} is the radius of the innermost stable circular orbit. The temperature of the disk lie between $10^5 - 10^2$ K with emission in the optical, UV to soft X-ray range according to Abramowicz and Straub 2023.

4.1.2 Corona and X-ray emission

From highly varying X-ray observations of AGN, it became indicative that there was a source of X-rays located close to the black hole. The most contemporary idea is that a corona of energetic particles is located above the accretion disk, and through inverse Compton scattering of the optical/UV photons that arise from the accretion disk produce the seen x-ray emission.

Inverse Compton scattering is the process of a photon gaining energy from a nearby relativistic particle. Due to the increase in efficiency of up scattering a photon with an electron compared to a proton, the corona x-ray emission is thought to be dominated by electrons. The process is as follows

$$e^- + \gamma \rightarrow e^- + \gamma \tag{20}$$

4.1.3 Broad and narrow line region

Broad emission lines in the case of AGN are formed from the high-density gas clouds located close to the central black hole. The high-density parameter is inferred from the fact that one only sees broad emission from permitted line transitions (e.g hydrogen Lyman and Balmer, iron, and magnesium). High densities allow for collisional de-excitation and in doing so prohibit so-called forbidden transitions. The broadening is an indication that these gas clouds are moving at huge velocities around the massive objects. This implies that they are located close to the black hole and receive the name the broad line region

Narrow emission lines are on the other hand formed in low-density gas clouds. The low densities are inferred from the fact that one sees both permitted and forbidden line transitions. They are narrow lines due to their velocities being substantially lower than the innermost gas clouds, and from here are thought to be located further away from the black hole, in the narrow line region.

4.1.4 Dust torus

The dust torus is a structure of dust that is thought to be located quite close to the black hole (0.1 - 10 pc). The main argument for the existence of this structure is the obscuration of the central region of the AGN. This obscuration is part of the unification scheme of AGN and was backed by the detection of polarized broad lines in AGN with their central core obscured. This polarization is what we would expect if some dust was obscuring the central region since the only light one sees is the light that is scattered into the line of sight Mason 2015. Further, studies on the dust torus have also revealed that the torus is not uniform but clumpy and quite dynamic with both in and outflows of matter depending on the state of the central engine Mason 2015.

4.1.5 Jets

A jet is a highly collimated outflow of plasma. The origin of the plasma is thought to be the accretion disk and the hot corona above it. These regions that have a high density of charged particles will under the influence of a magnetic field be accelerated and collimated into a jet-like structure. The energy mechanism which powers the jet is not fully understood, but the most prevalent theory is the Blandford-Znajek process. It says that the rotation of the accretion disk induces a magnetic field that will interact with a rotating black hole, effectively extracting energy from the black hole and supplying it to the jet. The jet structure extends far beyond the local area of the AGN maintaining a stable configuration over these distances. The classification of these jets is usually divided into two groups according to Walg et al. 2013, FRI and FRII. They are differentiated by their luminosity where FRI jets are less luminous and have a more diffuse structure while FRII jets are more luminous and have a more stable structure reaching further out. To add to this distinction it is thought that FRII jets are a product of an efficient accretion disk while FRI jets are a product of an inefficient accretion disk. This is discussed in Bian and Zhao 2003 where they show that radio quiet and Seyfert 1 galaxies have lower accretion efficiency while radio loud galaxies have higher accretion efficiency. Beyond the energy and their structure, the jets are also notable for their emission of non-thermal radiation such as synchrotron and inverse

Compton radiation.

4.2 Types of AGN

Before the unification of the AGN astronomers named the puzzling objects based on their observational properties. These names are still used to this day and are somewhat useful since their observational properties are important parameters for further study. The different classifications are important in understanding which objects could have the potential to produce the different observables one looks for in the night sky. Therefore, it seems appropriate to discuss some different types of AGN and their observational properties. The classification in this section is heavily based on Sanders 2021.

Type I and II AGN: One distinguishes type I and type II AGN based on the presence of broad emission lines. In other words, this distinction is a matter of a visible nucleus or not. Type I refers to sources whose nucleus is exposed to the observer and whose spectrum has both narrow and broad emission lines. Type II refers to sources whose nucleus is obscured by a torus and therefore mainly has narrow emission lines.

Blazars: The most extreme class of AGN. These sources are distinguished by their relativistic jets that are pointed towards the observer. This jet produces both synchrotron and Inverse Compton gamma rays and are extremely variable over short timescales. The emission is also highly polarized. Often and including in this report one divides Blazars into subgroups based on the emission lines. The two most common are BL Lacs and Flat spectrum radio quasars (FSRQs). The difference between the two is the presence of broad emission lines, where BL Lacs have no broad emission lines while FSRQs do. In addition, the distinction comes from the type of jet structure thought to be associated with the source. FRI jets for Bl Lacs and FRII for FSRQs.

Radio galaxies: Jetted AGN that as the name suggests these sources are very bright in the radio band. They usually refer to AGN viewed edge-on, where the torus might block the emissions from the accretion disk. The orientation of Radio galaxies gives way to strong synchrotron radiation, and they are often used to study the jet structure of AGN.

Seyfert galaxies: Spiral galaxies that have a bright nucleus. They are bright in the optical band and have a smaller active region than radio galaxies. They are often divided into two groups Seyfert I and Seyfert II where the distinction comes from type I and II. The galaxies also show quite high variability indicating a small emitting region.

Compton thin AGN: A way of distinguishing AGN that can be quite useful. These AGN have lower absorption compared to Compton-thick AGN, which allow more X-rays to escape making them easier to identify.

All these different distinctions are a help in understanding what processes one might be observing. The different dominant bands indicate different processes being in the line of sight, and by considering the modern structure of AGN one can then try to determine the underlying dynamics.

5 Luminosity functions

In this section, we will discuss the use of luminosity functions to characterize the populations of different AGN. A luminosity function (LF) is a function that maps the distribution of celestial bodies, like galaxies or quasars, based on their luminosity and corresponding comoving volume elements. These functions serve as a tool to understand the evolutionary patterns of these objects and allow us to predict the number density of these objects.

Typically, the focus is on the differential luminosity function, which is defined as

$$\frac{d\Psi(L,z)}{dL} = \frac{d^2N(L,V_c(z))}{dLdV_c(z)}. \tag{21}$$

One also can change the differential of the comoving volume into a term only depending on the redshift assuming the source population is isotropic and by multiplying with the differential comoving volume element. This transformation goes as follows,

$$\frac{d^2N(L,V_c(z))}{dLdV_c(z)}\frac{dV_c(z)}{dz} = \frac{N(L,z)}{dLdz}. \tag{22}$$

Several articles express the luminosity function in base 10 logarithm, and we note the conversion between the two:

$$\frac{d\Psi(L,z)}{dLog(L)} = \ln(10)L\frac{d\Psi(L,z)}{d(L)}. \tag{23}$$

To effectively determine the LF, it's typical to divided it into two distinct components: a local term and a time evolution term. This approach involves taking the local luminosity function, calculated at a redshift $z=0$, and then scaling it with a function that accounts for the change in redshift. The exact form of the total LF varies based on the source object, but it generally falls into two categories derived from the method of incorporating the growth term into the local LF. These methods are selected based on which best represents the observed evolution.

The two distinctions are the Pure Density Evolution (PDE) and the Pure Luminosity Evolution (PLE). The PDE model modifies the local density function to reflect changes over time, while the PLE model adjusts the local luminosity. The evolution is better represented by their equations and is given as

Parameter values for the X-ray luminosity functions

Model	LF params A	L_{star}	γ_1	γ_2	Evolution params v_1	v_2	z_c	L_c	α
SLDDE RG	8.375^a	2.138^b	2.15	1.10	4.00	-1.50	1.90	3.981^b	0.317
AMPLE-Blazar	1.379^a	1.81^b	-0.87	2.73	3.45	-0.25			
AMPLE-FSRQ	0.175^a	2.42^b	-50.0	2.49	3.67	-0.30			
APLE-BLlac	0.830^a	1.00^b	2.61		-0.79				
APLE-Seyfert	0.909^b	0.61^b	0.8	2.67					
ULDDE-CTN AGN^c	2.91^a	0.93^b	0.96	2.71	4.78	-1.5	1.86	4.07^b	0.29

Table 3: X-ray LF parameters, a, normalized by a factor of 10^{-7}, b, normalized by a factor of 10^{44} c, has more factors that do not fit in the table, $z_{c2} = 3$, $\alpha_2 = -0.1$, $L_{c2} = 10^{44}$, $v_3 = -6.2$, $\beta = 0.84$

Model Name	Luminosity Range	reference	No of objects
SLDDE RG	42 - 47	Silverman et al. 2008	682
AMPLE Blazar	43 - 49	Ajello et al. 2009	38
AMPLE FSRQ	45.5 - 49	Ajello et al. 2009	26
APLE BLlac	44.5 - 49	Ajello et al. 2009	12
APLE Seyfert	41 - 47	Ajello et al. 2009	199
ULDDE All CTN AGN	42 - 46	Ueda, Akiyama, Hasinger, et al. 2014	4452

Table 4: Luminosity range for different models, the luminosity range is given in log10.

$$\frac{d\Psi(L,z)}{d(L)} = \begin{cases} \frac{d\Psi(L/e(z),z=0)}{d(L)} & (PLE) \\ \frac{d\Psi(L,z=0)}{d(L)} e(z) & (PDE) \end{cases} . \tag{24}$$

Here one sees the common way of representing the luminosity functions. The local luminosity function is scaled by a factor of $e(z)$ which is the evolution term.

5.1 X-ray LF

For a given type of celestial object, different spectral bands will be more useful than others. In the case of AGN, the X-ray band is particularly significant. The reason of interest for X-ray production is that the correlation between the produced X-ray luminosity can possibly be used to infer some luminosity of the more elusive particles UHECRs and neutrinos. A simple argument for this is that the ingredients for this X-ray production in the corona (hot electrons) are thought to be accompanied by the ingredients for the production of UHECRs and neutrinos (charged ions).

Therefore, several studies have focused on defining the luminosity functions for classes of AGN with the X-ray spectrum.

In the following, I will define the X-ray luminosity functions for various AGN classifications, including Radio Galaxies, Seyfert Galaxies, and Blazars. Furthermore, an additional breakdown will consider FSRQs and BL Lacs within Blazars. In addition to this, a study by Ueda, Akiyama, Hasinger, et al. 2014 also looked at the total evolution of all Compton-thin AGN by combining multiple surveys and research. It will work as a reference point as well as describe the total evolution of these objects. The luminosity functions are collected from three papers Ajello et al. 2009 and Silverman et al. 2008, and Ueda, Akiyama, Hasinger, et al. 2014 and their form is explained below.

The local luminosity function:

The local luminosity function is the luminosity function at $z = 0$. The simplest form of the local luminosity function is expressed in Ajello et al. 2009 and is given as a power law. For our classes, it represents only the local LF for the class of BL Lacs and is given as

$$\frac{d\Psi(L, z = 0)}{dL} = \frac{A}{L}\left(\frac{L}{L_*}\right)^{1-\gamma_2} \tag{25}$$

This functional form has the fewest parameters and therefore suits well for populations that have few detected sources, but has the disadvantage of not being able to capture all the details of the observed local luminosity functions when source counts increase. For that reason a more complex local function is needed which was proposed in Ueda, Akiyama, Ohta, et al. 2003 and is described by a double power law. The double power law is used for the remaining classes of AGN and is given as follows

$$\frac{d\Psi(L, z = 0)}{dL} = \frac{A}{\log(10)}\frac{1}{L}\left(\left(\frac{L}{L_*}\right)^{\gamma_1} + \left(\frac{L}{L_*}\right)^{\gamma_2}\right)^{-1} \tag{26}$$

Evolution factor:

In addition to the local LF one also considers the evolution factor denoted $e(z)$. This factor captures the observed evolution of these objects and is the second part of the total luminosity function.

Again for the simplest evolution with the fewest parameters, a power law is used.

$$e(z) = (1 + z)^{v_1}$$

Certain situations necessitate a more detailed approach to the redshift evolution. As detailed in Ajello et al. 2009, a modified evolution is frequently employed. This adaptation transforms the conventional Pure Luminosity Evolution (PLE) and Pure Density Evolution (PDE) into their modified counterparts, namely Modified PLE (MPLE) and Modified PDE (MPDE). It is within these modified frameworks that a dependence on redshift z emerges in the exponent, providing a more nuanced understanding of the evolutionary processes involved. It is given as

$$e(z) = (1+z)^{v_1+v_2 z}$$

To expand further as described in Silverman et al. 2008 the evolution factor of the luminosity function is not always as simple as a modified power law only dependent on the redshift z. For some sources, a more complex evolution is needed. In Silverman et al. 2008 they use a double power law to better fit the data where the evolution is now not only dependent on the redshift but also on the luminosity. This then receives the apt name luminosity-dependent density evolution (LDDE) since it is a modified version of a (PDE) The functional form of the LDDE is as follows

$$e_z(z,L) = \begin{cases} (1+z)^{v_1} & \text{when} z \leq z_*(L) \\ e_z(z_*(L),L) \times \left(\frac{1+z}{1+z_*(L)}\right)^{v_2} & \text{when} z > z_*(L). \end{cases} \tag{27}$$

with $z(L)$ being defined as

$$z_*(L) = \begin{cases} z_c \left(\frac{L}{L_c}\right)^{\alpha} & \text{when} L \leq L_c \\ z_c & \text{when} L > L_c. \end{cases} \tag{28}$$

The expansion of the parameter space allows for easier fitting to the observed data, but comes of course with an increase in complexity and possible over fitting.

Lastly Ueda, Akiyama, Hasinger, et al. 2014 considered an XLF for the entire population of Compton thin AGN and naturally this has a more complex evolution structure. It is also an LDDE model but with three steps instead of two which we have in Silverman et al. 2008. The evolution is given as

$$e_z(z,L) = \begin{cases} (1+z)^{p_1} & \text{when} z \leq z_*(L) \\ (1+z_*)^{p_1}\left(\frac{1+z}{1+z_*(L)}\right)^{v_2} & \text{when} z > z_*(L) \\ (1+z_*)^{p_1}(\frac{1+z_{*2}}{1+z_*})^{v_2}(\frac{1+z}{1+z_{*2}})^{v_3} & \text{when} z > z_{*2}(L) \end{cases} \tag{29}$$

with the exponent p_1 being defined as

$$p_1 = v_1 + \beta(log(L) - 44) \tag{30}$$

with $z_*(L)$ being defined as

$$z_*(L) = \begin{cases} z_c \left(\frac{L}{L_c}\right)^{\alpha} & \text{when} L \leq L_c \\ z_c & \text{when} L > L_c \end{cases} \tag{31}$$

and $z_{*2}(L)$ being defined as

$$z_{*2}(L) = \begin{cases} z_{c2} \left(\frac{L}{L_{c2}}\right)^{\alpha_2} & \text{when} L \leq L_{c2} \\ z_{c2} & \text{when} L > L_{c2} \end{cases} \tag{32}$$

Armed with the functional form of the total luminosity function one can now fit the parameters to the observed data. This is done in Silverman et al. 2008, Ajello et al. 2009 and Ueda, Akiyama, Hasinger, et al. 2014 and their model name is similar as discussed in Jacobsen et al. 2015 which is a combination of the source paper (S, A, U), the type of model it describes (PLE, MPLE, LDDE) and the object in question. The parameters are then fitted to the data using a maximum likelihood method and the observational data of several X-ray surveys, see the cited papers for more information. One can see the parameters for the different models in table 3 and the luminosity range for which the different models are valid in table 4.

6 Luminosity function results

In this section, we will be using the different luminosity functions from the previous section to calculate the evolution of the different classes of AGN with redshift and also the distribution of AGN as a function of luminosity. By understanding these trends one can start understanding the nature of these objects, when they are created, and the amount of energy they release into the Universe.

6.1 Luminosity distribution

For the different classes discussed one can integrate the differential luminosity function over redshift to retrieve the Luminosity distribution of each object. This distribution highlights the difference in emitting power and therefore illuminates any trends that might be interesting. One calculates the luminosity distribution by multiplying the class-specific luminosity function with the differential comoving volume and integrating over the relevant redshift bin.

The luminosity distribution is given as

$$\frac{dN(L)}{dL} = \int_{z_{\min}}^{z_{\max}} \frac{\Psi(L, V(z))}{dL} \frac{dV(z)}{dz} dz \tag{33}$$

Here, $z_{\min}$ and $z_{\max}$ are the limits of the redshift bin. By separating it into bins of redshift one can assess how the class varies with redshift, and how a change in redshift would change the slope/trend of the distribution.

In Figure 6 one can see the luminosity density for the six different luminosity functions. The distribution is separated into four bins of redshift ($0 < z < 2, 2 < z < 4, 4 < z < 6, 6 < z < 8$). Further on in the report one will group our six classes into two groups based on observational properties, jet-dominated AGN and non-jet-dominated AGN. Jet-dominated AGN are the classes of Blazars, FSRQs, and Bl Lacs. Non-jet-dominated AGN are the classes of radio galaxies, CTN AGN, and Seyferts. The distinction comes from the orientation of the jet towards the observer discussed in section 4.

The most interesting feature of these distributions is the difference between the break luminosity between jet-dominated classes and non-jet-dominated classes. For two out of three jet-dominated classes the luminosity distribution peaks at a certain point and decreases on both sides. The breakpoint for Blazars and FSRQs indicates some preferred luminosity in which one finds the most sources. This preferred luminosity also seems consistent with different epochs. To investigate this

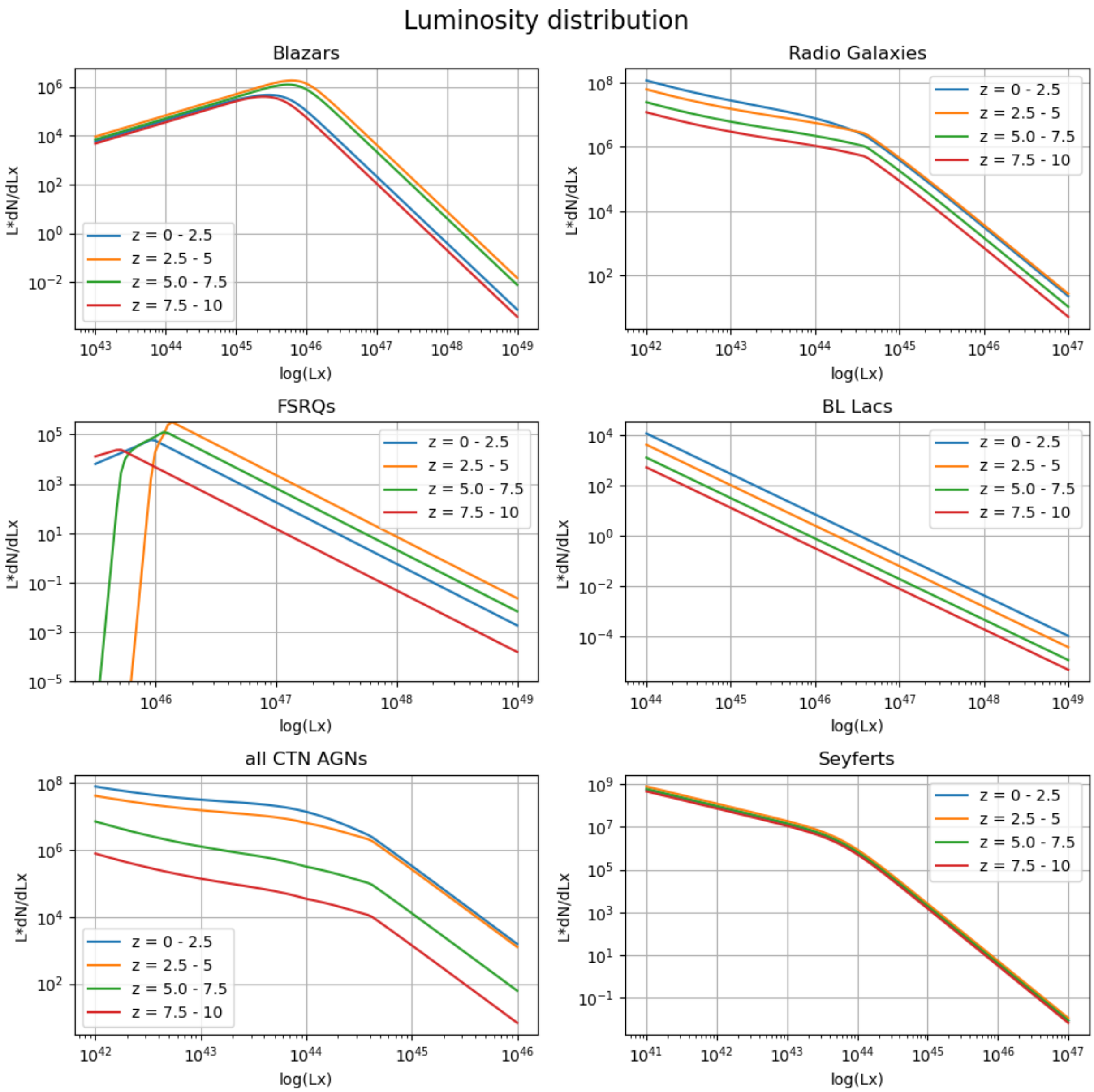

Figure 6: Luminosity distribution for the different classes of AGN. The different classes are defined in the title as well as the chosen LF model.

preferred energy one could investigate different optical bands and see if the same trend is observed. In Narumoto and Totani 2006 they discuss the luminosity function for Blazars but in the gamma ray band. The evolution function they use is a luminosity dependent density evolution similar to our radio galaxies and CTN AGN. They also find a peak in the luminosity distribution, this time at a higher luminosity than the one found here. Therefore, it could be that there is a distribution of Blazars that form around a certain luminosity since one sees this trend in the x-ray and gamma ray band. This is not necessarily true, and one should investigate the surveys used to see the correlation between x-ray and gamma ray selected AGN. The only exception to this is the BL Lacs which are represented as a simple power law and therefore have no break point in their distribution. With the inclusion of more BL Lacs in future data sets it would be interesting to see if this is still the case.

For the non-jet-dominated classes, one sees an increase in numbers towards lower energies similar to Bl lacs, but at some specific luminosity radio galaxies and CTN AGN introduce a break where the slope index changes. The break luminosity is very interesting and differentiate itself from jet-dominated AGN since it seems to show a breaking point where the creation of more powerful sources becomes less numerous. This breakpoint is also varying based on the redshift bin, where for higher redshift, the break is more sudden. For the Seyferts that have no evolution factor there is no distinction between lower or higher redshift. Any change in the slope of a power-law is cause for investigation since it seems to indicate some dynamic which might not be represented in our models. The softening of the break depending on redshift might indicate that this break is not as sudden as one would assume looking at higher redshift objects, but the change in slope index is still observed. The different interpretation of the luminosity distribution of these objects is fascinating and further study could illuminate why one would observe this difference, and if it is an effect of the sources or our observation of them. One notes these different reasons because the author of this paper has not found any explanation to why the number of our sources suddenly drop at a certain luminosity.

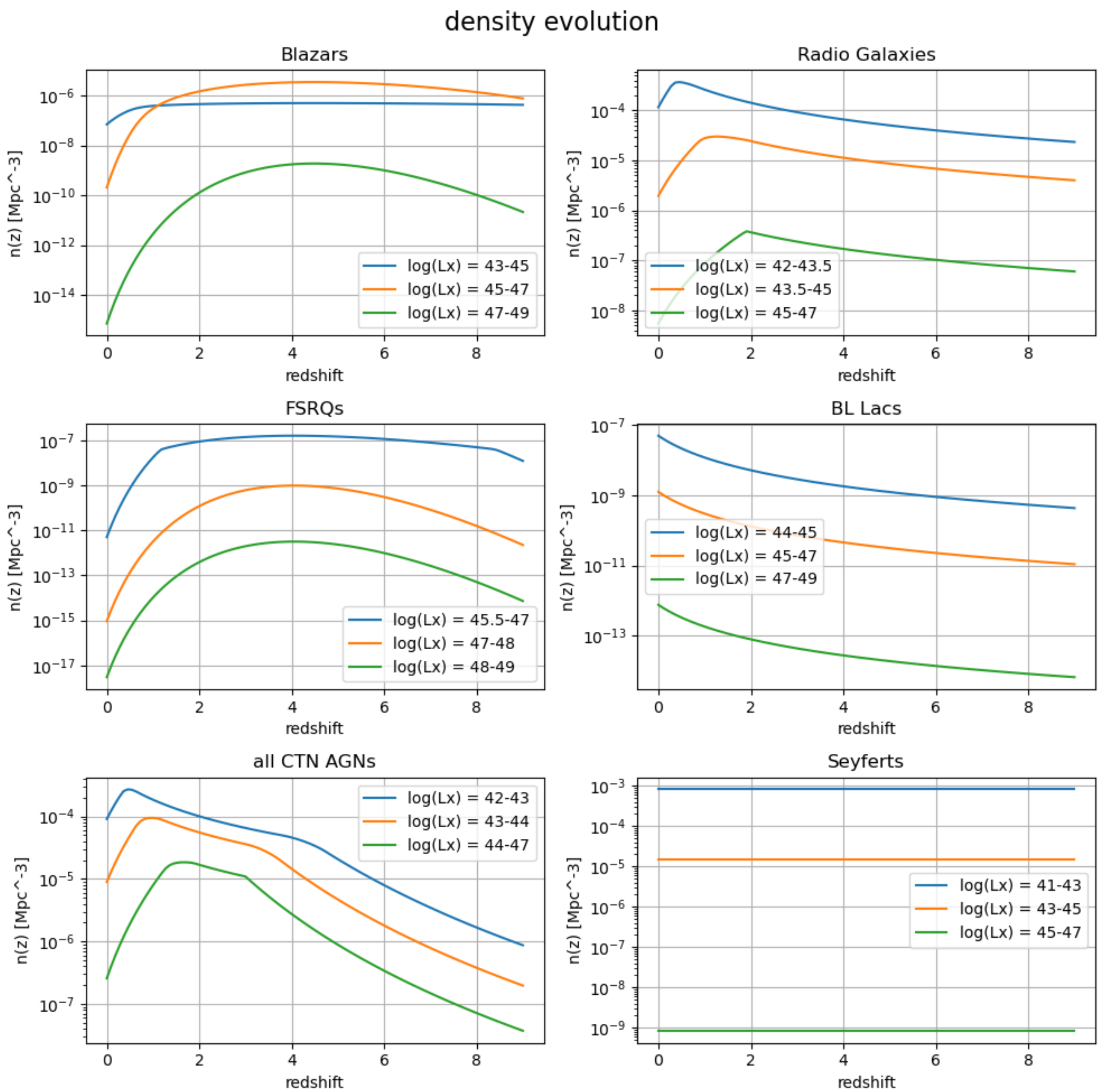

Figure 7: Density distribution for the four different classes of AGN. The different classes are defined in the title as well as the chosen LF model.

6.2 Density distribution

In addition to the luminosity distribution one can also calculate the number density of the different classes of AGN. This is done by integrating the differential luminosity function over luminosity. This will illuminate the evolution in time, or more precisely in redshift of the different classes. The integral is given as

$$n(z) = \frac{N(z)}{V(z)} = \int_{L_{\min}}^{L_{\max}} \frac{\Psi(L, V(z))}{dL} dL \tag{34}$$

Here again, we separate into luminosity bins to see the evolution of different parts of the luminosity distribution, most notably to see the difference before and after the break luminosity for most classes. The results can be seen in Figure 7

The density evolution of these objects is very interesting information due to it being closely tied to galaxy evolution. The evolution of Blazars and FSRQs differentiate themselves significantly from the other classes in figure 7 where both FSRQs and Blazars have a positive evolution with a peak in density around redshift $z = 5$. The total counterpart to this is the third class of jet-dominated AGN, the Bl Lacs. Here one sees a negative evolution with an increase in density in the more recent epochs. In a paper by Garofalo et al. 2019 he talks about the different evolutionary paths that generate the respective classes of Bl lacs and FSRQs which could be the origin of this discrepancy. While both classes belong to the parent class of Blazars the evolutionary path of FSRQs is thought to come from FRII radio galaxies while the evolutionary path of BL Lacs is from FRI radio galaxies. As mentioned in section 4.1.5 the difference between FRI and FRII jets is thought to be the accretion efficiency. In addition to this a paper by Bian and Zhao 2003 which studied the correlation between accretion rates and bolometric luminosity mentions that the nature of the central black hole and its rotation will have an effect on the accretion efficiency. Drawing from this one could indicate that the difference in evolution stems from the different evolutionary paths of their central engine, Kerr black hole or not. This is for the time being not an accepted explanation and still a topic of debate. Another try to explain how accretion efficiency is related to the central engine is in Raimundo et al. 2012 where they discuss a finding that showed the efficiency of the accretion being proportional to the mass of the black hole. More precisely they found this relation: $\eta \propto M^{0.5}$. Although this could help explain our density evolution of FSRQs and Bl Lacs by allowing FSRQs to host bigger black holes they also mentioned that this effect might be an artifact of the parameter space used. Lastly, one could also try to look at the evolution of material that can be accreted around the central black hole to possibly start unraveling the different evolutionary paths. From this it is only reasonable to conclude that this difference in evolution is captivating and is prone to an interesting answer.

For the Blazar population, one notices the same trend as for the luminosity distribution. The luminosity bin before the break luminosity stays more constant than the ones after the break. The reason for such an evolution would likely be tied to the same mechanism driving Bl lacs and FSRQs. Due to the decline of FSRQs, one should also expect the higher-end luminosity of Blazars to follow.

For the non-jet-dominated AGN, one finds a different story. Here the redshift peak, if any, is at around $z = 0.3$ where the peak is dependent on the luminosity bin. Lower luminosity AGN peaks at lower redshift. Therefore, the trend of density seems to be going toward lower-power radio galaxies and Compton-thin AGN. What is very interesting is comparing this evolution to the evolution of star formation. From Madau and Dickinson 2014 the star formation rate peaks at around 3.5 billion years after the Big Bang, or around redshift $z = 1.9$. This is in stark contrast to our sources where only the most luminous radio galaxies and Compton thin AGN peak at this redshift. The star formation rate then places itself in between the two peaks between jet-dominated and non-jet-dominated AGN which opens up for interpretation.

6.3 Expected luminosity

From the luminosity function, one can also calculate the expected luminosity of a source class at different redshifts. This is important since it will relate to the power injection of the different epochs and from this one can calculate an expected emissivity of the different classes of AGN. The expected luminosity of each group can be calculated with the following formula

$$\langle L \rangle = \frac{\int_{L_{\min}}^{L_{\max}} L \frac{\Psi(L,V(z))}{dL} \frac{dV(z)}{dz} dL}{\int_{L_{\min}}^{L_{\max}} \frac{\Psi(L,V(z))}{dL} \frac{dV(z)}{dz} dL} \tag{35}$$

furthermore, the emissivity which is a measure of energy per unit volume per unit time is given as

$$\epsilon = \int_{L_{\min}}^{L_{\max}} L \frac{\Psi(L,V(z))}{dL} \frac{dV(z)}{dz} dL \tag{36}$$

The different luminosity ranges are the same as before and are given in table 4. The results are shown in figure 8.

The expected luminosity is shown at the top in figure 8 where it shows the expected power output of the different classes. Here one sees that FSRQs are indeed the most luminous AGN and that they represent some of the most luminous objects in the Universe. The expected luminosity also shows the evolutionary trend of Blazars where they are now tending towards lower average luminosity. All classes remain fairly constant, but radio galaxies and CTN AGN both have a decline in expected luminosity after the star formation peak at $z = 1.9$. This could be inferred from figure 7 but is more clearly seen here.

The emissivity of each class as a function of redshift is shown in figure 8 at the bottom. Here it shows a change in dominance between Blazars and our CTN and radio galaxies. This change that happens around redshift $z = 1$ is a result of the different evolutionary paths of our sources seen in figure 7.

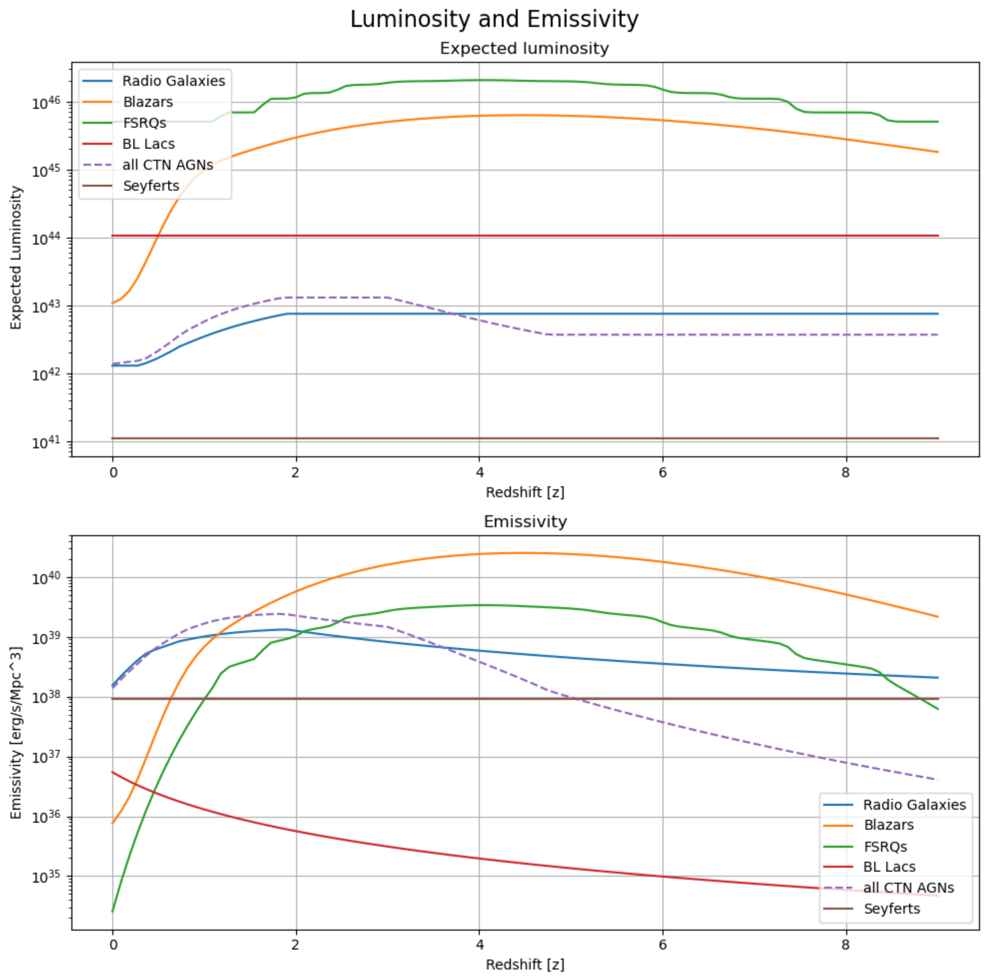

Figure 8: Expected luminosity and emissivity for the different classes of AGN.

7 AGN power injection estimation

7.1 UHECRs emissivity

With the calculated emissivity for the different groups there is now the possibility to look from an energy budget viewpoint into the possibility of AGN being the sources of UHECRs. By ignoring the method of acceleration, but considering that our sources must produce the required emissivity one can make a crude estimation of source candidates.

From the calculation in 3.2.3 the emissivity of UHECRs is given as $9.2 \cdot 10^{44}$erg/Mpc^3/yr this was calculated from the observed flux of UHECRs from the Pierre Auger observatory Collaboration et al. 2017. In this calculation, one needed to confine the area in which these sources could be produced to take into account the energy losses these particles experience. The same argument must be used for our emitting sources and therefore one must use the emissivity of our sources at a redshift very close to Earth. To get a comparable emissivity one evaluates therefore the emissivity at redshift $z = 0.01$. The result is shown in figure 2

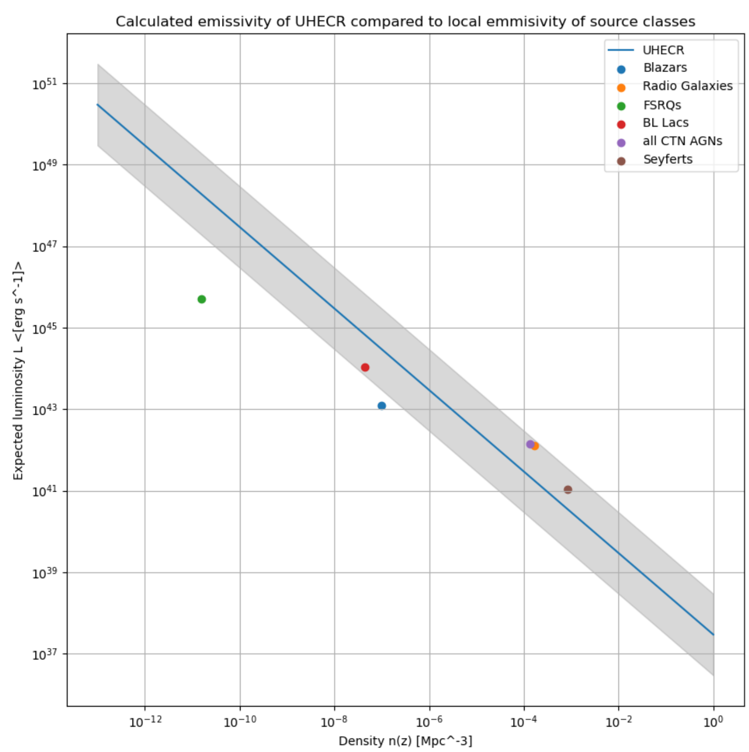

Figure 9: UHECR emissivity for the different classes of AGN.

This figure shows that most classes of AGN produce a total emissivity in X-ray comparable to the one detected by the Pierre Auger observatory. The only exceptions are the FSRQs and Blazars which are not numerous enough or powerful enough at this redshift. To criticize this very crude estimate, one must first note that the correlation between X-ray luminosity and UHECR luminosity is not well-defined and should include parameters that are not accounted for. In addition to this, one has not done any separation between jet-dominated and non-jet-dominated AGN, and even though our non-jet-dominated AGN are capable of producing the required X-ray luminosity the mechanism of transferring this energy into UHECRs is not well understood.

Nevertheless, the result does not rule out the possibility of AGN being the origin of the UHECR diffuse flux.

7.2 Neutrino emissivity

Similarly, for the UHECRs, we calculated the local emissivity for the neutrinos in section 3.3.3. The result was $1.2 \cdot 10^{44}\text{erg/Mpc}^3/\text{yr}$ which is a factor similar to that of UHECRs. In the calculation, the diffuse neutrino flux on Earth was taken from the IceCube observatory Abbasi et al. 2022 and the energy range was taken to be $1\text{TeV} - 10\text{PeV}$ corresponding to the astrophysical neutrino flux detected by IceCube. The difference between the UHECR flux to the neutrino flux is the energy loss mechanism. The effect of a very limited energy loss mechanism means that the emitting area is now the whole universe. To reach a comparable emissivity one must therefore take a redshift-dependent average of the sources over the whole universe. One does this by scaling the emissivity at redshift z with the corresponding energy loss for a neutrino from that redshift given as $(1 + z)$ and then taking the average emissivity to get a comparable emissivity. The resulting figure is shown in figure 10.

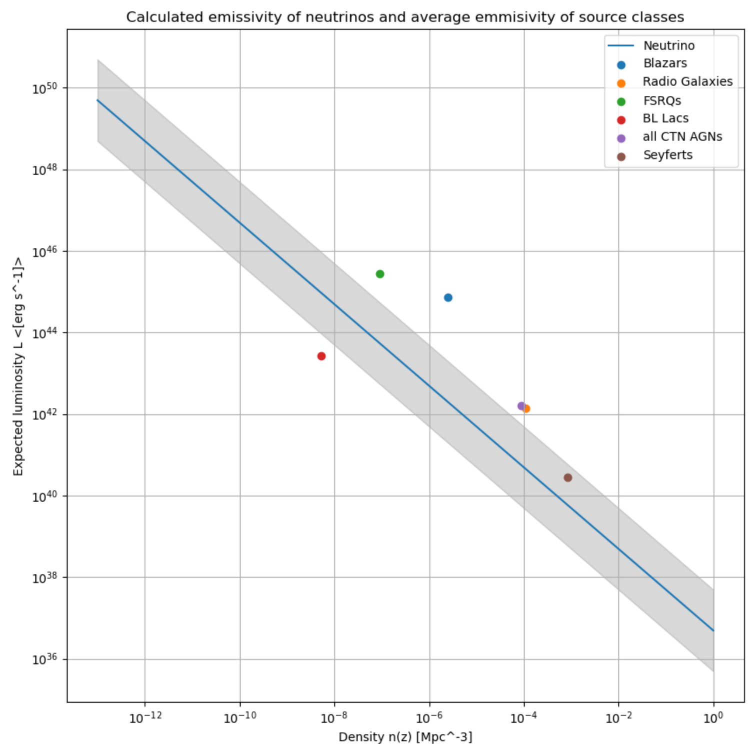

Figure 10: Neutrino emissivity for the different classes of AGN.

This figure shows that the neutrino flux can be produced by all classes except the BL Lacs. This is an effect of the averaging since the BL lacs have a negative evolution.

In addition to the average picture given in figure 10 one can also calculate the expected diffuse neutrino flux directly from the different classes of AGN. This is done by modifying a transfer function defined in Palladino et al. 2020, and it is given as

$$\frac{d\phi_\nu}{dE_\nu} = \int_0^{z_{max}} \frac{D_H}{E(z)} \frac{L(E_\nu(1+z), < L_x > (z))}{(1+z)^2} \rho(z) dz \tag{37}$$

Here D_H is the Hubble distance, $E(z)$ is the function defined in section 2.4, $L(E_\nu(1+z), < L_x > (z))$ is a power law representing the neutrino flux at the source, which when integrated reproduces the average source luminosity at redshift z, and $\rho(z)$ is the number density of the sources at redshift z. With this function, we can calculate the expected diffuse flux of neutrinos from the sources. The difference between Palladino et al. 2020 and this work, is the inclusion of a luminosity dependence in the power-law function. This is done to account for the different average luminosity of the different classes of AGN which was assumed constant in Palladino et al. 2020. The assumption of a constant luminosity is not a bad one since the luminosity of the different classes is not changing significantly over the redshift range, but it is still a simplification, especially for the Blazar class. The form of the power law representing the neutrino flux is taken to be identical to the model used for the astrophysical neutrino flux by IceCube which is defined in section 3.3.3. The result is shown in figure 11.

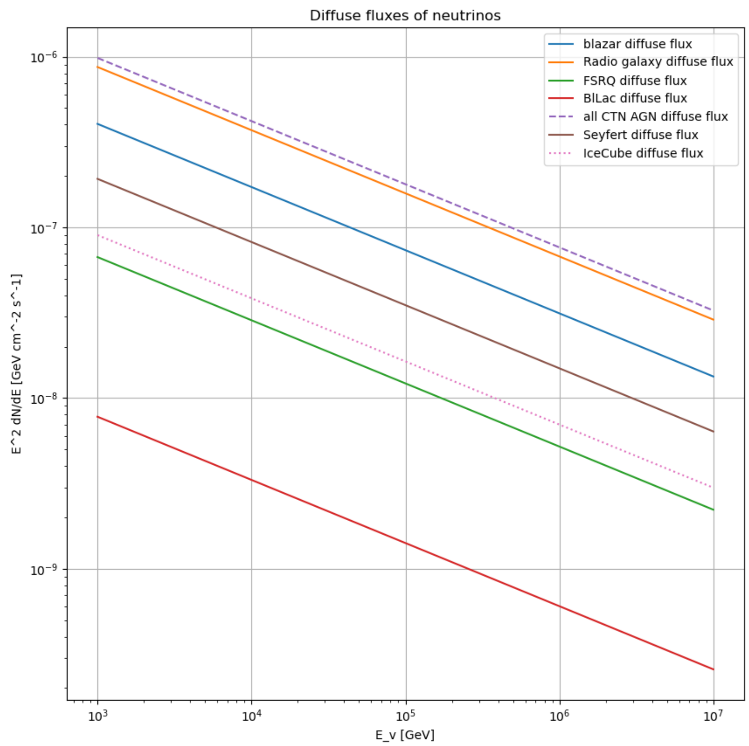

Figure 11: Diffuse neutrino flux for the different classes of AGN.

What one sees here is almost the same result as the crude average which is good. The FSRQs and Bl lacs are now not able to produce the diffuse flux but the rest are. The fact that most sources are overshooting the observed neutrino flux would be a problem if we had a more constrained solution. Any model that overshoots could not be the source since it is not what we observe, but in our case, our solution rests on the fact that the neutrino luminosity is equal to the X-ray, a simple assumption. Therefore, the only concrete conclusion one can draw from this is that the neutrino flux can be produced by the AGN since they can produce the required emissivity, if one lets the X-ray luminosity be equal the neutrino luminosity.

This result in figure 11 is obtained differently than in figure 10 and therefore the agreement between them is a good sign. The argument that the X-ray luminosity should have the same value as the neutrino luminosity is not a bad first guess, but it does leave a lot to be desired. This flux model does not incorporate any parameters of the AGN other than emitting strength, and therefore it is not a very nuanced model. In order to incorporate the observational properties of AGN, one could model the acceleration of particles and consequently their direction. This would give different fluxes for different classes of AGN and one can argue this by looking at current acceleration models. Two possible ways of accelerating particles which compliments the different classes discussed in this report is the Blandford-Znajek process which produces jets, and outflow mechanics which can in theory take any direction but are usually discussed as outflows into the plane of the host galaxy. For jet-dominated AGN the most accepted theory of energy extraction from rotating black holes is discussed in Blandford and Znajek 1977. This method of acceleration which is produced by ordered electric fields drives the accelerated particles into jets. One cares about this since any emission of particles especially neutrinos would therefore be highly pointed and one would only expect AGN with a jet pointed in our line of site to produce neutrinos we would detect. Outflows as discussed in Laha et al. 2021 is another way of accelerating particles. The problem one faces here is then the uncertainty of accelerating our particles enough. The mechanism of outflow is not certain enough to produce the highest energy UHECRs and neutrinos. The orientation of these outflows can be also be difficult to determine therefore it becomes harder to use these outflows as consistent methods of generating our desired particles. What this example aims to show is that a model of acceleration and emission direction could heavily constrain which class of AGN could produce the observed neutrino flux.

Nevertheless, what this crude model can show is that these objects do produce enough power. An additional source of improvement without doing much more work is to look at the gamma-ray luminosity functions of the same sources and see if they can produce the required neutrino flux. Gamma-ray production is a natural consequence of pion decay and also leads to neutrino production. In this way, one could more easily constrain the neutrino production with the gamma-ray production. This is however outside the scope of this report and will be left for future work.

8 Conclusion

8.1 Summary

In this report I have modelled the evolution of different classes of AGN, and calculated their emissivity of UHECRs and neutrinos based on X-ray luminosity functions. This emissivity was then compared to the emissivity of UHECRs and neutrinos measured at Earth.

For the distribution over luminosity one finds that Blazars and FSRQs both have a peak luminosity which is dependent on redshift around $10^{45.5}$erg. One also discusses that the peak luminosity seen in Blazars is also seen in the luminosity function from a survey in the gamma ray band, which could highlight an intriguing area of additional research. Conversely, Bl Lacs show an increase in numbers towards lower luminosity. Similarly, non jet-dominated AGN also show the same trend as Bl lacs, but with a break luminosity around $10^{44.5}$erg where the slope index changes. One argues that the break luminosity in non-jet-dominated AGN is an interesting artifact illuminating a breaking point in which these sources become harder to either detect or produce, and that it warrants further investigation.

Regarding the redshift evolution one finds that Blazars and FSRQs show a peak in their density around $z = 5$ with the brightest changing the most. In contrast, Bl Lacs show a negative evolution with redshift being the only AGN to do so. Non jet-dominated AGN peak around $z = 0.5$ where the peak is dependent on luminosity. The exception is Seyferts which in our chosen model is constant with redshift. The differences in evolution between Bl Lacs and FSRQs while being from the same class is discussed but yields no concrete answers, suggesting a new area for further research to understand these discrepancies.

By also modelling the emissivity of our AGN one finds a change between the biggest energy injectors around redshift $z = 1$. Before this redshift the biggest energy injectors were Blazars, while after it was surpassed by radio galaxies and Compton thin AGN. This result illuminates the fact also seen in the density evolution, that the "golden age" of Blazars is passed.

Lastly, when looking at emissivity estimates of our AGN one finds that almost all classes of AGN can alone produce the observed diffuse flux of UHECRs and neutrinos. For UHECRs it is only FSRQs that cannot produce enough energy in X-ray to explain the observed flux. For neutrinos, it is only Bl Lacs that cannot produce enough energy in X-ray to explain the observed flux. On also tries to estimate the diffuse flux of neutrinos with a transfer model, and with this model one finds that both FSRQs and Bl lacs lie beneath the observed diffuse flux of neutrinos. One concludes that one needs a better correlation between X-ray luminosity, neutrinos luminosity and UHECR luminosity in order to receive a more concrete answer on the emissivity of UHECRs and neutrinos.

In addition, a huge caveat in the results of emissivity is the fact that we have not included the observational properties of AGN, most notably jet orientation. The conclusion of this result is that AGN can be a source of UHECRs and neutrinos, but it does leave a lot to be desired.

8.2 Future outlook

The results of this report do highlight some very interesting features in the luminosity function of X-ray selected AGN. The break luminosity in non-jet-dominated AGN can be a hint to a type of boundary in which these sources become harder to produce. Any further exploration of this feature would maybe need to look for the same feature in other bands, and preform a correlation analysis between the AGN selected for the different bands. What's more, the correlation between the luminosity function of Blazars in the X-ray band and the gamma ray band is also an interesting feature that could yield some interesting results.

In regard to the emissivity estimates it became clear to the author early on that a more detailed model was needed to be made to receive a less vague answer. In still rings true that AGN can be a source of UHECRs and neutrinos, but further expansion on the transfer model which includes the orientation, and the class of AGN could create a more satisfying answer. It would be interesting to create an acceleration model for particles located in the X-ray corona and then propagating them through the AGN and try and capture the dynamics one might imagine happening.

References

Aab, A. et al. (Sept. 2020). "Features of the Energy Spectrum of Cosmic Rays above 2.5 Using the Pierre Auger Observatory". In: *Phys. Rev. Lett.* 125 (12), p. 121106. DOI: 10.1103/PhysRevLett.125.121106. URL: https://link.aps.org/doi/10.1103/PhysRevLett.125.121106.

Abbasi, R. et al. (Mar. 2022). "Improved Characterization of the Astrophysical Muon–neutrino Flux with 9.5 Years of IceCube Data". In: *The Astrophysical Journal* 928.1, p. 50. DOI: 10.3847/1538-4357/ac4d29. URL: https://dx.doi.org/10.3847/1538-4357/ac4d29.

Abdul Halim, A. et al. (2023). "Constraining the sources of ultra-high-energy cosmic rays across and above the ankle with the spectrum and composition data measured at the Pierre Auger Observatory". In: *Journal of Cosmology and Astroparticle Physics* 2023.05, p. 024. ISSN: 1475-7516. DOI: 10.1088/1475-7516/2023/05/024. URL: http://dx.doi.org/10.1088/1475-7516/2023/05/024.

Abramowicz, Marek A. and Dr. Odele Straub (2023). *Accretion Discs.* 3.12.2023. URL: http://www.scholarpedia.org/article/Accretion_discs.

Ajello, M. et al. (2009). "THE EVOLUTION OF SWIFT/BAT BLAZARS AND THE ORIGIN OF THE MeV BACKGROUND". In: *The Astrophysical Journal* 699.1, p. 603. DOI: 10.1088/0004-637X/699/1/603. URL: https://dx.doi.org/10.1088/0004-637X/699/1/603.

Alves Batista, Rafael et al. (June 2019). "Open Questions in Cosmic-Ray Research at Ultrahigh Energies". In: *Frontiers in Astronomy and Space Sciences* 6. ISSN: 2296-987X. DOI: 10.3389/fspas.2019.00023. URL: http://dx.doi.org/10.3389/fspas.2019.00023.

Andeen, Karen and Matthias Plum (Jan. 2019). "Latest Cosmic Ray Results from IceTop and IceCube". In: *EPJ Web of Conferences* 210, p. 03005. DOI: 10.1051/epjconf/201921003005.

Andrews, Henrik (2023). *Master project.* URL: https://github.com/henan99/Master-Project.

Bian, Wei-Hao and Yong-Heng Zhao (June 2003). "Accretion Rates and the Accretion Efficiency in AGNs". In: *Publications of the Astronomical Society of Japan* 55.3, pp. 599–603. ISSN: 0004-6264. DOI: 10.1093/pasj/55.3.599. eprint: https://academic.oup.com/pasj/article-pdf/55/3/599/17447902/pasj55-0599.pdf. URL: https://doi.org/10.1093/pasj/55.3.599.

Blandford, R. D. and R. L. Znajek (July 1977). "Electromagnetic extraction of energy from Kerr black holes". In: *Monthly Notices of the Royal Astronomical Society* 179.3, pp. 433–456. ISSN: 0035-8711. DOI: 10.1093/mnras/179.3.433. eprint: https://academic.oup.com/mnras/article-pdf/179/3/433/9333653/mnras179-0433.pdf. URL: https://doi.org/10.1093/mnras/179.3.433.

Collaboration, The Pierre Auger et al. (2017). *The Pierre Auger Observatory: Contributions to the 35th International Cosmic Ray Conference (ICRC 2017).* arXiv: 1708.06592 [astro-ph.HE].

Dermer, Charlees D. and Govind Menon (2009). *High Energy Radiation from Black Holes: Gamma Rays, Cosmic Rays, and Neutrinos.* Princeton University Press.

Garofalo, David et al. (Jan. 2019). "The redshift distribution of BL Lacs and FSRQs". In: *Research in Astronomy and Astrophysics* 19.1, p. 013. ISSN: 1674-4527. DOI: 10.1088/1674-4527/19/1/13. URL: http://dx.doi.org/10.1088/1674-4527/19/1/13.

Hillas, A. M. (1984). "The Origin of Ultra-High-Energy Cosmic Rays". In: *Annual Review of Astronomy and Astrophysics* 22.1, pp. 425–444. DOI: 10.1146/annurev.aa.22.090184.002233. URL: https://doi.org/10.1146/annurev.aa.22.090184.002233.

Hogg, David W. (2000). *Distance measures in cosmology.* arXiv: astro-ph/9905116 [astro-ph].

Jacobsen, Idunn B. et al. (2015). "High-energy neutrino fluxes from AGN populations inferred from X-ray surveys". In: *Mon. Not. Roy. Astron. Soc.* 451.4, pp. 3649–3663. DOI: 10.1093/mnras/stv1196. arXiv: 1506.05916 [astro-ph.HE].

Kotera, Kumiko and Angela V. Olinto (2011). "The Astrophysics of Ultrahigh-Energy Cosmic Rays". In: *Annual Review of Astronomy and Astrophysics* 49.1, pp. 119–153. DOI: 10.1146/annurev-astro-081710-102620. eprint: https://doi.org/10.1146/annurev-astro-081710-102620. URL: https://doi.org/10.1146/annurev-astro-081710-102620.

Laha, Suvendu et al. (Jan. 2021). "Ionized outflows from active galactic nuclei as the essential elements of feedback". In: *Nature Astronomy* 5.1, pp. 13–24. ISSN: 2397-3366. DOI: 10.1038/s41550-020-01255-2. URL: https://doi.org/10.1038/s41550-020-01255-2.

Madau, Piero and Mark Dickinson (Aug. 2014). "Cosmic Star-Formation History". In: *Annual Review of Astronomy and Astrophysics* 52.1, pp. 415–486. ISSN: 1545-4282. DOI: 10.1146/annurev-astro-081811-125615. URL: http://dx.doi.org/10.1146/annurev-astro-081811-125615.

Mason, Rachel E (2015). "Dust in the torus of the AGN unified model". In: *Planetary and Space Science* 116. Cosmic Dust VII, pp. 97–101. ISSN: 0032-0633. DOI: https://doi.org/10.1016/j.pss.2015.02.013. URL: https://www.sciencedirect.com/science/article/pii/S0032063315000483.

Narumoto, Takuro and Tomonori Totani (May 2006). "Gamma-Ray Luminosity Function of Blazars and the Cosmic Gamma-Ray Background: Evidence for the Luminosity-Dependent Density Evolution". In: *The Astrophysical Journal* 643.1, pp. 81–91. ISSN: 1538-4357. DOI: 10.1086/502708. URL: http://dx.doi.org/10.1086/502708.

Netzer, Hagai (2015). "Revisiting the Unified Model of Active Galactic Nuclei". In: *Annual Review of Astronomy and Astrophysics* 53.1, pp. 365–408. DOI: 10.1146/annurev-astro-082214-122302. URL: https://doi.org/10.1146%2Fannurev-astro-082214-122302.

Palladino, Andrea et al. (Apr. 2020). "Can astrophysical neutrinos trace the origin of the detected ultra-high energy cosmic rays?" In: *Monthly Notices of the Royal Astronomical Society* 494.3, p. 4255 4265. ISSN: 1365-2966. DOI: 10.1093/mnras/staa1003. URL: http://dx.doi.org/10.1093/mnras/staa1003.

Raimundo, S. I. et al. (Jan. 2012). "Can we measure the accretion efficiency of active galactic nuclei?" In: *Monthly Notices of the Royal Astronomical Society* 419.3, pp. 2529–2544. ISSN:

0035-8711. DOI: 10.1111/j.1365-2966.2011.19904.x. eprint: https://academic.oup.com/mnras/article-pdf/419/3/2529/18717746/mnras0419-2529.pdf. URL: https://doi.org/10.1111/j.1365-2966.2011.19904.x.

Sanders, Nathan (2021). *Guide to Classification of Galaxies and AGNs.* 15.11.2023. URL: https://astrobites.org/guides/galaxy-and-agn-types/.

Shields, Gregory A. (1999). "A Brief History of Active Galactic Nuclei". In: *Publications of the Astronomical Society of the Pacific* 111.760, pp. 661–678. DOI: 10.1086/316378. URL: https://doi.org/10.1086%2F316378.

Silverman, J. D. et al. (May 2008). "The Luminosity Function of X-Ray-selected Active Galactic Nuclei: Evolution of Supermassive Black Holes at High Redshift". In: *The Astrophysical Journal* 679.1, p. 118. DOI: 10.1086/529572. URL: https://dx.doi.org/10.1086/529572.

Stanev, Todor (June 2009). "Propagation of ultrahigh-energy cosmic rays". In: *New Journal of Physics* 11.6, p. 065013. DOI: 10.1088/1367-2630/11/6/065013. URL: https://dx.doi.org/10.1088/1367-2630/11/6/065013.

Ueda, Yoshihiro, Masayuki Akiyama, Günther Hasinger, et al. (Apr. 2014). "TOWARD THE STANDARD POPULATION SYNTHESIS MODEL OF THE X-RAY BACKGROUND: EVOLUTION OF X-RAY LUMINOSITY AND ABSORPTION FUNCTIONS OF ACTIVE GALACTIC NUCLEI INCLUDING COMPTON-THICK POPULATIONS". In: *The Astrophysical Journal* 786.2, p. 104. DOI: 10.1088/0004-637X/786/2/104. URL: https://dx.doi.org/10.1088/0004-637X/786/2/104.

Ueda, Yoshihiro, Masayuki Akiyama, Kouji Ohta, et al. (2003). "Cosmological Evolution of the Hard X-Ray Active Galactic Nucleus Luminosity Function and the Origin of the Hard X-Ray Background". In: *The Astrophysical Journal* 598.2, p. 886. DOI: 10.1086/378940. URL: https://dx.doi.org/10.1086/378940.

Walg, S. et al. (June 2013). "Relativistic AGN jets I. The delicate interplay between jet structure, cocoon morphology and jet-head propagation". In: *Monthly Notices of the Royal Astronomical Society* 433.2, pp. 1453–1478. ISSN: 0035-8711. DOI: 10.1093/mnras/stt823. eprint: https://academic.oup.com/mnras/article-pdf/433/2/1453/4923906/stt823.pdf. URL: https://doi.org/10.1093/mnras/stt823.